STRUCTURAL BIOLOGY

Structural insight into UV-B–activated UVR8 bound to COP1

Yidong Wang[1]†, Lixia Wang[1]†, Zeyuan Guan[1]†, Hongfei Chang[1], Ling Ma[1], Cuicui Shen[1], Liang Qiu[1], Junjie Yan[1], Delin Zhang[1], Jian Li[2], Xing Wang Deng[2,3]*, Ping Yin[1]*

The CONSTITUTIVE PHOTOMORPHOGENIC 1-SUPPRESSOR OF PHYA-105 (COP1-SPA) complex is a central repressor of photomorphogenesis. This complex acts as an E3 ubiquitin ligase downstream of various light signaling transduced from multiple photoreceptors in plants. How the COP1-SPA activity is regulated by divergent light-signaling pathways remains largely elusive. Here, we reproduced the regulation pathway of COP1-SPA in ultraviolet-B (UV-B) signaling in vitro and determined the cryo-electron microscopy structure of UV-B receptor UVR8 in complex with COP1. The complex formation is mediated by two-interface interactions between UV-B-activated UVR8 and COP1. Both interfaces are essential for the competitive binding of UVR8 against the signaling hub component HY5 to the COP1-SPA complex. We also show that RUP2 dissociates UVR8 from the COP1-SPA4$^{1–464}$-UVR8 complex and facilitates its redimerization. Our results support a UV-B signaling model that the COP1-SPA activity is repressed by UV-B-activated UVR8 and derepressed by RUP2, owing to competitive binding, and provide a framework for studying the regulatory roles of distinct photoreceptors on photomorphogenesis.

INTRODUCTION

Light is a key environmental factor critical for plant growth and development (*1*–*3*). Plants perceive different wavelengths of light through distinct photoreceptors and mediate light responses to initiate photomorphogenesis or light-driven plant growth (*1*–*5*). Various proteins play important roles in the light-signaling networks, of which the E3 ubiquitin ligase COP1 (CONSTITUTIVE PHOTOMORPHOGENIC 1) acts as a pivotal repressor of plant photomorphogenesis (*1*–*9*). It forms complexes with SPAs (SUPPRESSOR OF PHYA-105) and can be further recruited by CULLIN4-Damaged DNA Binding Protein1 (CUL4-DDB1-COP1-SPAs) to target and destabilize HY5 (ELONGATED HYPOCOTYL 5; a key regulator playing versatile roles in nearly all light-signaling pathways) and other transcriptional regulators of photomorphogenesis (*8*, *10*–*17*). COP1 and SPAs are closely related proteins comprising three domains that are connected through flexible linkers (*1*, *6*, *8*, *14*, *15*, *18*). Of the three domains, two are the coiled-coil domain in the middle and the Tryptophan-Aspartic acid 40 (WD40) domain at the C terminus; the remaining one is the Really Interesting New Gene (RING) finger domain and kinase-like domain at the N-termini in COP1 and SPAs, respectively (fig. S1A) (*1*, *6*, *8*, *14*, *15*, *18*). It has been suggested that specific Val-Pro (VP) peptide motifs commonly exist in COP1-interacting transcription factors and act as the binding sites to the WD40 domain of COP1 (COP1^{WD40}) (*1*, *6*, *19*). On the other hand, multiple light-activated photoreceptors, such as ultraviolet B (UV-B) light receptor [UV RESISTANCE LOCUS 8 (UVR8)] and the blue light receptors [cryptochrome 1 and 2 (CRY1/CRY2)], use VP peptide motifs to interact with the COP1-SPA complex and suppress its activity by outcompeting their signaling components from degradation, thereby initiating photomorphogenesis (*1*, *3*, *6*, *20*, *21*).

In UV-B–induced photomorphogenesis, COP1 exerts its function through direct interaction with UVR8 (*1*–*3*, *20*, *22*–*24*). UVR8 is a β-propeller protein tailed with a flexible C-terminal domain (fig. S1A) (*2*, *25*–*27*). The N-terminal β-propeller domain [regulator of chromosome condensation 1 (RCC1)-like core domain] is mainly responsible for UV-B perception and homodimer formation, and the C-terminal domain contains a VP motif that is crucial for UV-B signaling (*2*, *25*–*29*). In UV-B signaling, homodimeric UVR8 converts to an active monomer upon UV-B exposure (*25*–*27*). Activated monomeric UVR8 interacts with the COP1-SPA complex, competitively inhibiting the degradation of its target proteins, such as HY5, inducing downstream UV-B signaling (*2*, *20*, *22*–*24*, *27*, *29*–*31*). Two WD40 proteins, RUP1 (REPRESSOR OF UV-B PHOTOMORPHOGENESIS 1) and RUP2, directly interact with UVR8 to facilitate its redimerization and inactivation (Fig. 1A) (*32*–*34*). Previous studies have revealed the structures of apo or VP motif–bound COP1^{WD40} and proposed that photoactivated photoreceptors, such as UVR8 and CRY2, compete with their signaling components for COP1^{WD40} binding via two distinct interfaces and with high-affinity binding (*20*, *35*). However, the molecular mechanisms underlying the regulation of the COP1-SPA complex activity by the light-activated photoreceptor remain largely elusive, mainly owing to the daunting challenges of the obtainment of the COP1-SPA complex.

RESULTS

Reconstitution of the UV-B signaling pathway

To obtain COP1-SPA complexes, we first coexpressed COP1 with different SPAs (SPA1 to SPA4) in the human embryonic kidney (HEK) 293F cell system, respectively. COP1-SPA4 showed a relatively higher level of expression compared to the other combinations (fig. S1B). However, the yield of the COP1-SPA4 complex was still low and not suitable for structure determination. To solve this

[1]National Key Laboratory of Crop Genetic Improvement, Hubei Hongshan Laboratory, Huazhong Agricultural University, Wuhan 430070, China. [2]Key Laboratory of Molecular Design for Plant Cell Factory of Guangdong Higher Education Institutes, Institute of Plant and Food Science, School of Life Sciences, Southern University of Science and Technology, Shenzhen 518055, China. [3]School of Advanced Agricultural Sciences and School of Life Sciences, State Key Laboratory of Protein and Plant Gene Research, Peking-Tsinghua Center for Life Sciences, Peking University, Beijing 100871, China. *Corresponding author. Email: yinping@mail.hzau.edu.cn (P.Y.); deng@pku.edu.cn (X.W.D.)
†These authors contributed equally to this work.

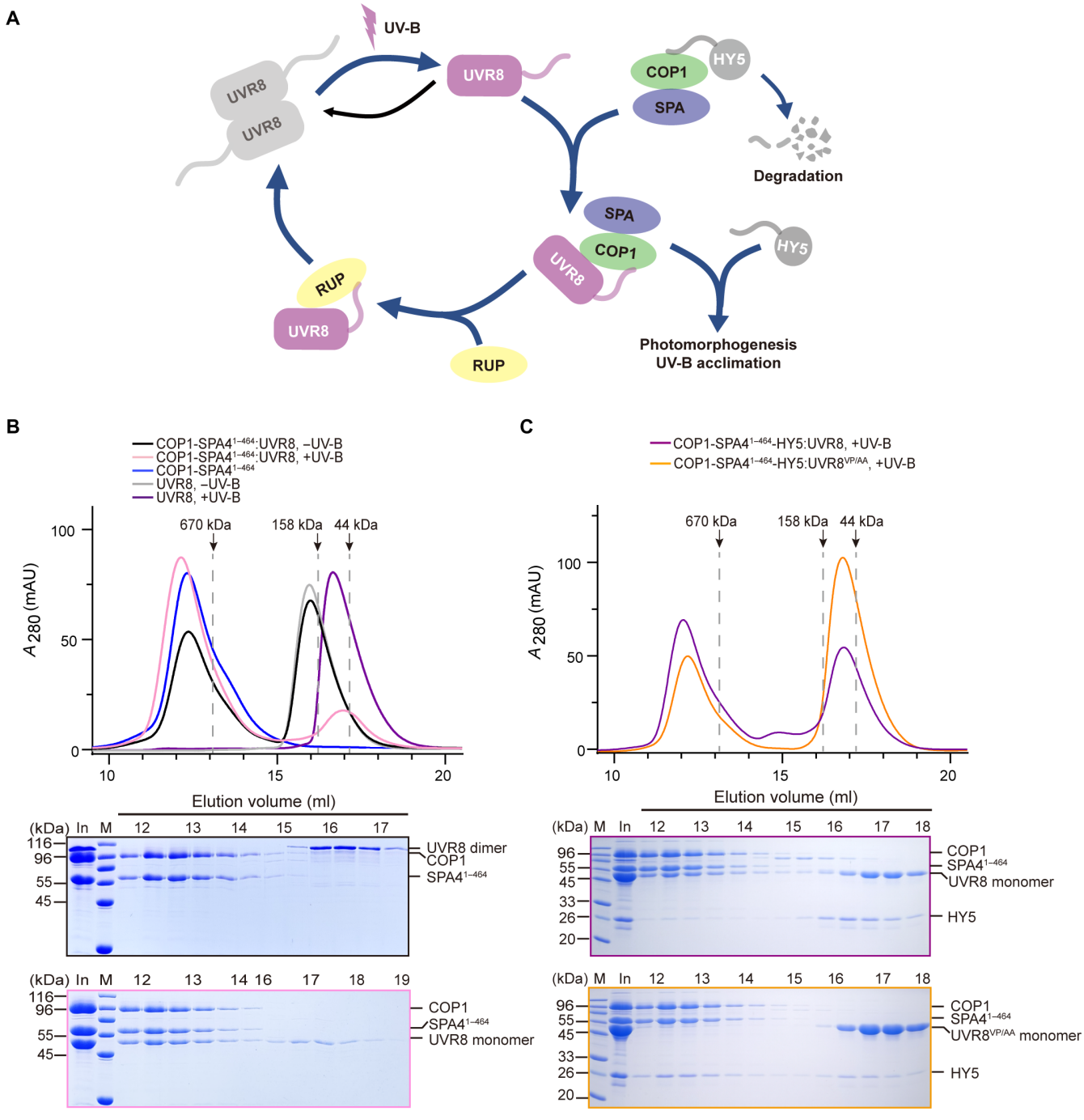

Fig. 1. Reconstitution of the COP1-SPA4$^{1–464}$-UVR8–mediated UV-B signaling pathway. (**A**) A schematic diagram of the core UVR8 photocycle. UVR8 exists as homodimers in the absence of UV-B. Upon UV-B exposure, homodimeric UVR8 converts to active monomer. Activated monomeric UVR8 interacts with the E3 ligase COP1-SPA complex, competitively inhibits the degradation of its target proteins, such as HY5, and induces downstream UV-B signaling. RUP1 and RUP2 (represented by RUP) directly interact with UVR8 to facilitate its redimerization and inactivation. For simplicity, the schematic drawing of COP1-SPA represents the oligomeric form of the complex. (**B**) Reconstitution of the COP1-SPA4$^{1–464}$-UVR8 complex is indicated by a representative gel filtration chromatography (pink lines). Lines in blue, dark, gray, and purple are representative gel filtration chromatography for the COP1-SPA4$^{1–464}$ complex, the COP1-SPA4$^{1–464}$ complex, UVR8 without UV-B treatment, and UVR8 with or without UV-B treatment, respectively. The estimated molecular weight of the COP1-SPA4$^{1–464}$-UVR8 complex is slightly larger than 670 kDa. Bottom: The SDS–polyacrylamide gel electrophoresis (SDS-PAGE) of the peak fractions for the COP1-SPA4$^{1–464}$ complex and UVR8 with or without UV-B treatment. (**C**) Competitive binding assay of COP1-SPA4$^{1–464}$-HY5 using UV-B–treated UVR8 (purple) or UVR8$^{VP/AA}$ mutant (orange). mAU, milli–absorbance units. M, molecular weight ladder (kDa). In, Input.

problem, we performed protein engineering on SPA proteins. We first removed the WD40 domain of SPAs and coexpressed the modified SPAs with COP1. All the truncated SPA proteins formed stable complexes with COP1, of which the COP1-SPA4$^{1–464}$ combination showed the highest yield (fig. S1C). Thus, this combination was chosen for further studies.

We then attempted to reconstitute the core UVR8 photocycle in vitro. UVR8 was extensively studied and well expressed in *Escherichia coli* (*25*, *26*). Consistent with previous reports (*17*, *31*), our gel filtration analysis showed that COP1-SPA4$^{1–464}$ only forms a stable and homogeneous complex with the UV-B–activated UVR8, but not with the UVR8 homodimer in the ground state (Fig. 1B). We also obtained HY5 in *E. coli* and reconstituted the COP1-SPA4$^{1–464}$-HY5 complex (fig. S2A). UV-B–activated UVR8 outcompeted HY5 from the COP1-SPA4$^{1–464}$-HY5 complex to some extent (Fig. 1C). The UVR8$^{VP/AA}$ mutant (alanine substitutions for the residues V410 and P411 in C27 subregion of UVR8) that was reported previously could not affect the COP1-HY5 interaction in yeast cells (*20*). Consistent with this, little UV-B–activated UVR8$^{VP/AA}$ mutant bound to COP1-SPA4$^{1–464}$, and only trace amount of HY5 was crowded out (Fig. 1C and fig. S2A). These results are consistent with the previous report that UV-B–activated UVR8 has higher affinity to COP1 than HY5 (*20*).

Overall structure of COP1^{WD40}-UVR8

We obtained the homogeneous COP1-SPA4$^{1–464}$-UVR8 complex and used it for cryo–electron microscopy (cryo-EM) sample preparation (detailed in Materials and Methods). After cryo-EM analysis, the structure of the COP1-SPA4$^{1–464}$-UVR8 complex was determined at an average resolution of ~3.1 Å. The density for the UVR8 core domain, COP1^{WD40}, and VP motif of UVR8 binding to COP1^{WD40} was observed, while the N-terminal domains of COP1 and SPA4 were missing, probably because of flexibility (Fig. 2, A and B, and fig. S3). Overall, COP1^{WD40}-UVR8 formed a heterodimer with a height of ~70 Å and a width of ~50 Å. The two central axes of the UVR8 core domain and COP1^{WD40} form an angle of approximately 45° (Fig. 2C). Superposition of the VP motif–bound COP1^{WD40} from this study and the previous report [Protein Data Bank (PDB), 6QTQ] reveals an almost identical overall structure with a root mean square deviation (RMSD) of 0.38 Å over 288 Cα atoms (fig. S4). The UVR8 core domain also displays conformational similarity to those from the previously reported wild-type/mutant UVR8s (fig. S8).

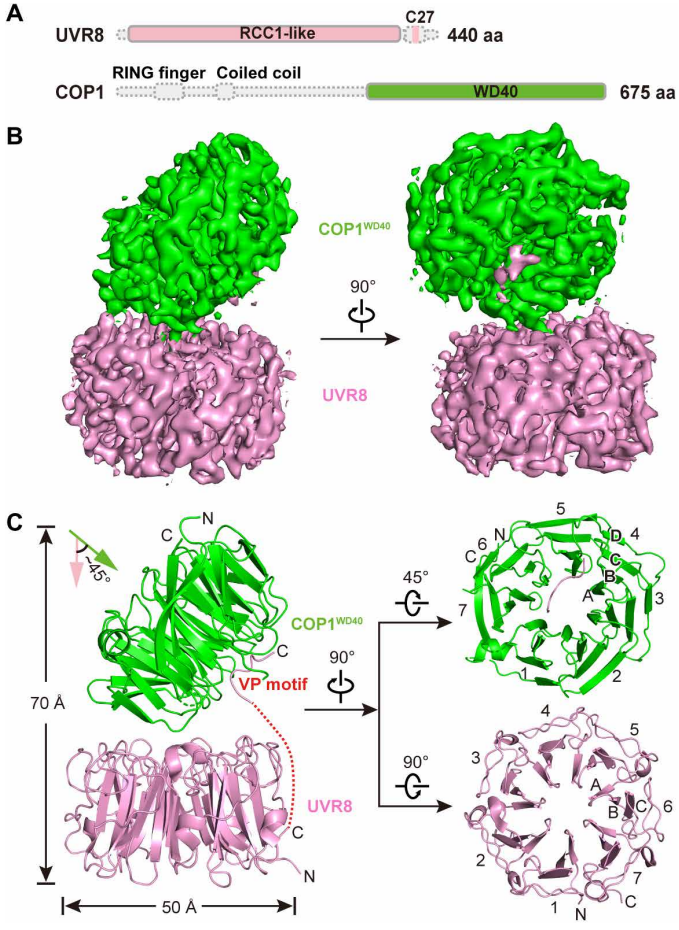

Fig. 2. Overall structure of the COP1^{WD40}-UVR8 complex. (**A**) Schematic representation showing the domain architectures of UVR8 and COP1. The RCC1-like core domain (core domain) and VP motif in the C-terminal domain of UVR8 are shown in pink. COP1 WD40 domain is colored green. Unresolved regions are indicated by dotted lines. aa, amino acids. (**B**) Views of the cryo-EM maps of the COP1^{WD40}-UVR8 complex, with the same color scheme as (A). (**C**) Overview of the COP1^{WD40}-UVR8 complex (left) and top view (right) of VP motif–bound COP1^{WD40} (top) and UVR8 core domain (bottom). Unresolved linkers of the C-terminal subregion of UVR8 are indicated by red dotted lines.

Two distinct interfaces mediated the interactions between COP1 and UVR8

The interactions between UVR8 and COP1 are mainly mediated through two interfaces, interface I and II (Fig. 3A), with a buried surface area of approximately 1399 Å^2. The VP motif of UVR8 makes contacts with the central hollow cavity of COP1 through hydrophobic and hydrophilic interactions as previously reported and forms interface I (Fig. 3, A and C, and figs. S4 and S6A). Both UVR8$^{1–396}$ (C-terminal truncation of UVR8; residues 1 to 396) and UVR8$^{VP/AA}$ reduced the binding of UV-B–activated UVR8 to COP1-SPA4$^{1–464}$ (fig. S5). These results suggest that the C27 subregion containing the VP motif is crucial for the interaction between COP1-SPA4$^{1–464}$ and UV-B–activated UVR8.

Interface II is located at the UVR8 core domain and the side face of COP1^{WD40}, which is mediated by an interaction network of salt bridges and hydrogen bonds between two patches of complementary charges (Fig. 3, B and C, and fig. S6). Specifically, E442, T452, E458, E460, and E463 in the COP1 negatively charged surface patch interact with UVR8 positively charged residues R338, R200, R234, R286, and K304, respectively. S392, R393, S418, R420, and R453 from the basic surface patch of COP1 interact with R146 (D44 and D77), Q148, D129, and N149 within the acidic surface patch of UVR8, respectively (Fig. 3C and fig. S6A). To our surprise, most of the UVR8 residues that are involved in the formation of interface II have been implicated in UVR8 UV-B perception and dimerization (*25*, *26*). The importance of these residues was supported by alanine substitutions and subsequent pull-down assays (fig. S6). UVR8^{D44A}, UVR8^{D129A}, UVR8^{R234A}, UVR8^{R286A}, UVR8^{K304A}, and UVR8^{R338A} showed markedly reduced binding affinity to COP1-SPA4$^{1–464}$, whereas UVR8^{R146A} and UVR8^{R200A} partially retained binding to COP1-SPA4$^{1–464}$. In contrast, D77A, Q148A, and N149A mutations in UVR8 had little impact on UVR8's binding to COP1-SPA4$^{1–464}$ (fig. S6B). R420A, E460A, and F595A in COP1 sharply influenced the interaction

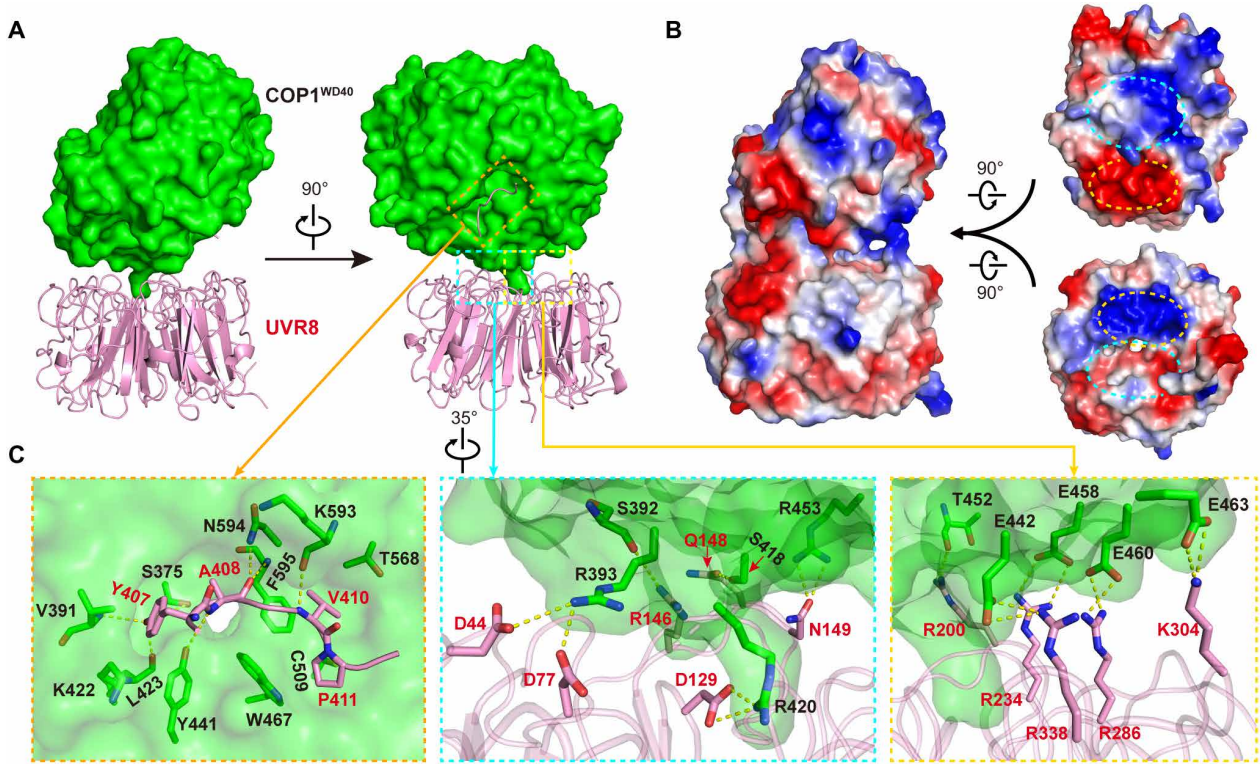

Fig. 3. Two distinct interfaces mediate the interaction between COP1 and UVR8. (**A**) Overview of the COP1^{WD40}-UVR8 complex. COP1^{WD40} and UVR8 (core domain and VP motif) were shown in surface and cartoon, respectively. Interface I was indicated by an orange dashed box, and interface II was indicated by cyan and gold dashed boxes. (**B**) The core domain of UVR8 interacts with COP1^{WD40} via two complementary charged surfaces, at which two patches with opposite electric charges are located. The negatively charged patch at the bottom of UVR8 interacts with the positively charged patch from COP1 (in cyan), and vice versa (in gold). (**C**) Close-up views of COP1^{WD40}-UVR8 interfaces indicated by colored dashed boxes in (A). Hydrogen bonds and salt bridges are indicated by yellow dashed lines.

between COP1-SPA4$^{1-464}$ and UVR8, whereas COP1^{R393A}, COP1^{Y441A}, COP1^{E442A}, and COP1^{E458A} partially retained binding to UVR8. Other COP1 mutants retained binding ability to UVR8 (fig. S6C). Combinational mutations of D44A/D77A/D129A, R234A/R286A/R338A, or R146/R200A showed further reduced binding affinity to COP1-SPA4$^{1-464}$ compared to singular mutants (fig. S6D). In line with this, UVR8^{D44A,D77A,D129A} and UVR8^{R234A,R286A,R338A} lost the ability to outcompete HY5 from the COP1-SPA4$^{1-464}$-HY5 complex (fig. S2B).

R420 from COP1 protrudes and inserts into the central hollow cavity of UVR8 core domain and interacts with D129 from UVR8 through both a salt bridge and a hydrogen bond (Fig. 3C). To further investigate the role of this residue, we mutated R420 to A, K, and E and examined the interaction of UVR8 with these COP1 variants. COP1^{R420K} partially retained binding ability to UVR8. In contrast, COP1^{R420A} and COP1^{R420E} presented markedly reduced binding affinity to UVR8 (fig. S7). These results suggest that R420 of COP1 is crucial for the interaction of COP1 and UVR8.

Structural feature of UV-B–activated UVR8

To further characterize the conformation of UV-B–activated UVR8, we compared the core domain structure of UV-B–activated UVR8 with those of wild-type UVR8 and UVR8^{W285A}, a proposed constitutively activated variant showing a constitutive activation phenotype in vivo (*26*, *31*). Superpositions of the structure of UV-B–activated UVR8 with wild-type UVR8 and UVR8^{W285A} revealed a nearly identical overall conformation (with RMSD values of 0.463 over 326 and 0.45 over 328 Cα atoms, respectively) (fig. S8). Given that the Trp triad (W233, W285, and W337) are critical for UV-B perception and the adjoining Arg residues (R146, R234, R286, and R338) and three aromatic amino acids (W250, Y253, and W302), K252, and D129 play important roles in the formation of UVR8 homodimer or the UVR8-COP1 complex (*25*, *26*), we examined whether these residues display any difference in configuration under different conditions.

Compared to ground-state wild-type UVR8, the side chains of these residues in UV-B–activated UVR8 undergo orientation shift (Fig. 4, A to D). The orientation alteration is especially evident for the Trp triad. All these Trps rotate to the opposite orientation against the axle of central hollow cavity, which results in the enlargement of the cavity. The Args adjoining to these Trps and the D129 have varying degrees of orientation alternations. As a result, the intramolecular cation-π interactions between these Trps and Args are completely disrupted (Fig. 4, C and D). These results suggest a crucial role of the cation-π interactions in the maintenance of the UVR8 homodimer.

UVR8^{W285A} and ground-state UVR8^{WT} exhibit a nearly identical structure except for notable side-chain alterations in residues D129, W233, and W337 (*26*). In contrast, superposition of the UV-B–activated UVR8 from the UVR8-COP1 complex with UVR8^{W285A} reveals vast changes of side-chain configurations in the abovementioned residues, indicating that UVR8^{W285A} is not the fully activated

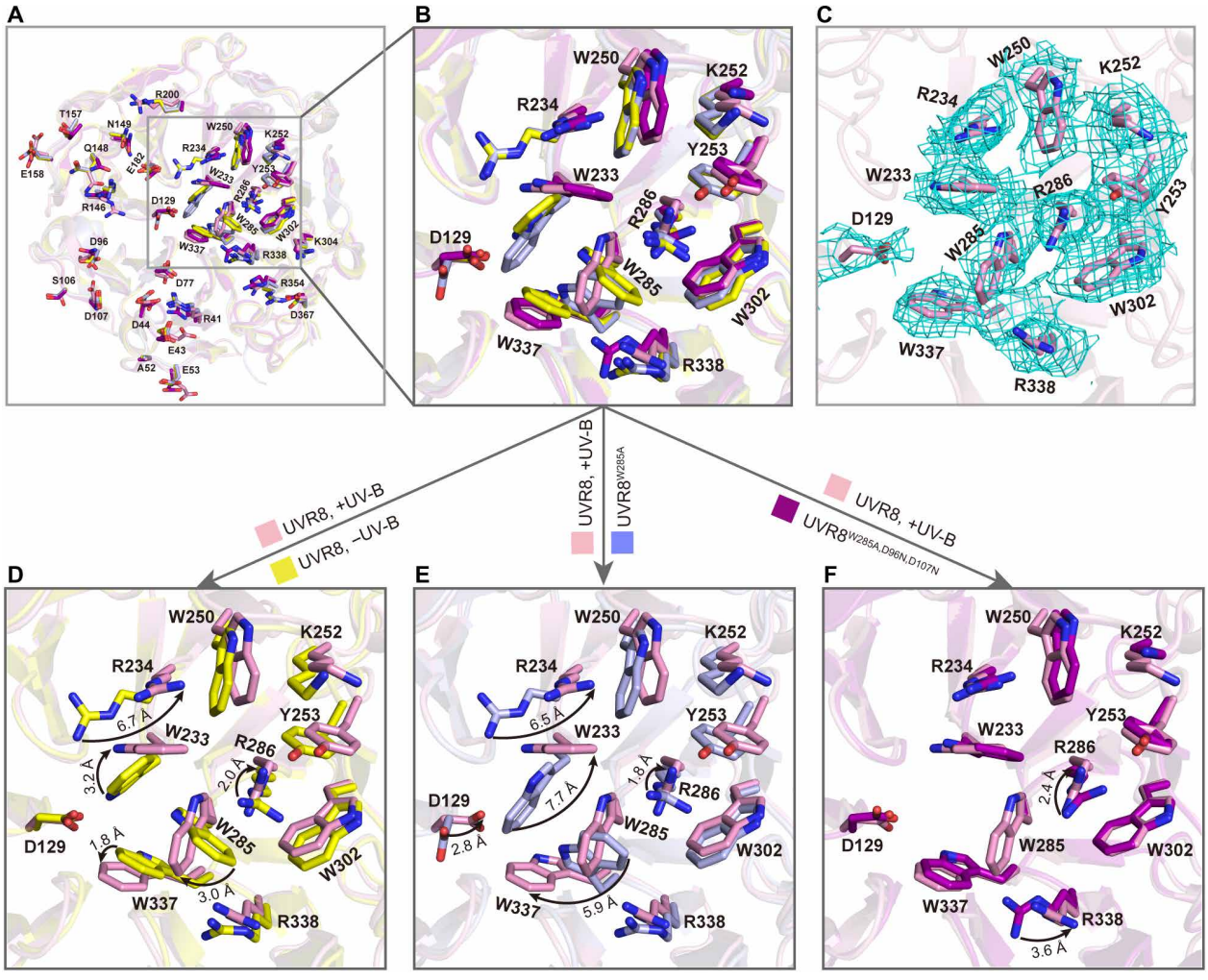

Fig. 4. Structural analyses of UV-B–activated UVR8. (**A** and **B**) Overview (A) and close-up view (B) of superposition of core domains from UV-B–treated UVR8 (UVR8, +UV-B; in pink) with a subunit of UVR8 without UV-B treatment (UVR8, –UV-B; in yellow; PDB: 4DNW), UVR8^{W285A} (in light blue; PDB: 4DNU), and UVR8^{W285A,D96N,D107N} (in magenta; PDB: 6XZM). (**C**) Cryo-EM density for the side chains of the residues that are involved in the cation-π interactions and dimerization in the UVR8, +UV-B structure. (**D** to **F**) Structural comparison of the core domains from UV-B–treated UVR8 with a subunit of UVR8 without UV-B treatment (D), UVR8^{W285A} (E), or UVR8^{W285A,D96N,D107N} (F). Residues involved in the cation-π interactions and dimerization were analyzed and shown in sticks. Distances were measured in PyMOL.

form of UVR8 (Fig. 4E). Recently, it was reported that combination of UVR8^{W285A} with D96N/D107N (UVR8^{W285A,D96N,D107N}) or G101S (UVR8^{W285A,G101S}) would strongly enhance the constitutive photomorphogenesis phenotype in plant and the binding affinity with COP1^{WD40} (*32*). Superpositions of the UV-B–activated UVR8 with UVR8^{W285A,D96N,D107N} also reveal a similar structural arrangement yet with smaller RMSD value (0.397 over 324 Cα atoms) compared to that of the UVR8^{W285A} (0.45 over 328 Cα atoms) or UVR8^{D96N,D107N} (0.42 over 324 Cα atoms) (fig. S8). Nearly all the above-analyzed residues in UVR8^{W285A,D96N,D107N} show similar configurations to these in UV-B–activated UVR8 (Fig. 4F). The dimeric UVR8^{W285A,D96N,D107N} in the crystal lattice exhibits similar structural features to COP1^{WD40}-UVR8 (fig. S9, A to D) (*32*). The interface of the unconventional homodimer is similar to interface II of UVR8-COP1. Moreover, R346 from one monomer inserts into the central hollow cavity of the other one (fig. S9E). The G101S mutation in UVR8 leads to the distortion of the loop harboring D96 and D107 and affects the stability of the UVR8 homodimer (*32*). Thus, it is reasonable to infer that UVR8^{W285A,G101S} and UVR8^{W285A,D96N,D107N} are similar variants representing the activated monomeric UVR8. In concert with this, these two mutants show comparable binding affinity to COP1^{WD40} in a constitutive manner to the native wild-type UVR8 treated with UV-B (*32*). These results strongly suggest that UVR8^{W285A,D96N,D107N} and UVR8^{W285A,G101S} may represent activated monomeric UVR8 variants.

RUP2 dissociates UVR8 from the COP1-SPA4$^{1–464}$-UVR8 complex and facilitates its redimerization

RUPs are closely related to COP1 and function in facilitating UVR8's redimerization (fig. S10) (*33*, *34*). UVR8-COP1 interaction was inhibited by overexpression of RUP2 in vivo (*33*). However, how RUP2 inhibits the UVR8-COP1 interaction remains elusive. The AlphaFold-predicted structure of RUP2 WD40 domain (RUP2^{WD40}) shows an architecture similar to that of COP1^{WD40} (RMSD = 0.8, over 224 Cα atoms) (fig. S11A). After docking of the predicted RUP2^{WD40} into that of the COP1^{WD40}-UVR8 complex, the five

conserved residues mediating the interaction between UVR8 and COP1 were also present at a similar location in the corresponding surface of RUP2^{WD40} (fig. S11, B to E). We replaced these residues and three other key charged residues on the surface of RUP2^{WD40} with alanine and examined the interaction between RUP2 mutants and UVR8^{W285A}, which forms a stable complex with RUP2 (*31*). Alanine substitutions of the conserved residues in RUP2 disrupted their binding to UVR8^{W285A} (fig. S12, A to C). In contrast to the wild-type RUP2 that could facilitate the redimerization of UVR8, the RUP2 mutants that cannot bind to UVR8 lost their facilitative function (fig. S12, D and E). We also performed competitive combination assay, in which the wild-type or mutant RUP2 was incubated with the COP1-SPA4$^{1–464}$-UVR8 complex, to analyze RUP2's role in the inhibition of the UVR8-COP1 interaction. The wild-type RUP2 successfully dissociates UVR8 from the COP1-SPA4$^{1–464}$-UVR8 complex and facilitates its redimerization (fig. S13A). As expected, RUP2 mutants containing mutations affecting the interaction with UVR8 showed little impact on the UVR8 dissociation/redimerization progress (fig. S13B). These results suggest that RUP2 outcompetes UVR8 from interacting with COP1-SPA4$^{1–464}$, probably due to higher binding affinity.

DISCUSSION

Previous studies have reported that a competitive photoreceptor-COP1-substrate tripartite interaction plays a crucial role in regulating common photoresponses in plants (*20*, *21*). Here, our structural and biochemical data provide substantial insights into the targeting mechanisms underlying the COP1 signaling pathways regulated by different photoreceptors. Specifically, UV-B–activated UVR8 outcompetes its signaling component HY5 for binding to COP1-SPA and forms the COP1-SPA-UVR8 complex. RUP2 subsequently outcompetes COP1-SPA and dissociates UVR8 from the COP1-SPA-UVR8 complex, facilitating the dimerization of the monomeric UVR8 (fig. S14). Unfortunately, we did not trace the N terminus of COP1 and SPA4, which mediates ubiquitination, possibly because of structural flexibility. The molecular mechanism of COP1-SPA ubiquitin ligase activity remains to be investigated in the future.

In this study, the recombinant COP1-SPA4$^{1–464}$ appears to be an oligomer based on the gel filtration chromatography profile (Fig. 1B). This is in line with previous reports that the full-length COP1-SPA4 forms an ~700-kDa oligomeric complex in vivo (*15*). COP1 is a RING E3 ubiquitin ligase, of which the RING domain has a direct role in binding the E2 ubiquitin-conjugating enzymes (*1*, *6*). Previous studies suggested that RING E3 ligases' oligomerization may promote their catalytic activity (*36*, *37*). Specifically, the oligomerization of E3s [for instance, baculoviral IAP repeat containing 7 (BIRC7), cellular inhibitor of apoptosis protein 2 (cIAP2), tumor necrosis factor receptor (TNFR)-associated factor 6 (TRAF6), RING finger protein 4 (RNF4), and murine double minute 2-murine double minute x (MDM2-MDMX)] can facilitate ubiquitylation in trans and/or enhance E3s' affinity to E2 ubiquitin-conjugating enzymes (*38*–*45*). We speculate that the oligomerization of COP1-SPA may also promote the enzymatic activity of the E3 ligase complex. In addition, COP1-SPA4$^{1–464}$-UVR8 has a larger size than the presumable oligomeric COP1-SPA4$^{1–464}$ in gel filtration analysis (Fig. 1B), suggesting that UVR8 binding has little effects on the COP1-SPA4 oligomerization throughout the UV-B signaling pathway. No in vitro and/or in vivo evidence for COP1-SPA–mediated UVR8 ubiquitination/degradation is currently available (*22*, *46*). The functional significance of COP1-SPA oligomerization in the context of UVR8 function remains to be investigated.

To avoid exaggerated light-activated response, plants also use additional regulators, RUP1 and RUP2, to negatively regulate UV-B signaling. RUP2 is closely related to the WD40 domain of COP1 (*34*). RUP2 and COP1 possibly bind to UVR8 via similar interacting surfaces. Collectively, these suggest that the UVR8-RUP2 interaction is probably similar to that of UVR8-COP1. It was reported that RUP1/RUP2 can be recruited by CUL4-DDB1 and form the UV-B–inducible E3 CUL4-DDB1-RUP1/RUP2 complex, which targets HY5 for proteolysis (*47*). Conversely, to stabilize HY5, RUP1 and RUP2 were targeted and degraded by COP1 (*47*). These findings have significantly advanced our knowledge of the orchestration of the UV-B signaling cascades. Further investigations are needed to elucidate the molecular basis underlying the facilitation of UVR8 redimerization and HY5 proteolysis by RUP1/2 and the molecular mechanism underpinning the COP1-mediated degradation of RUP1/2.

MATERIALS AND METHODS

Molecular cloning and protein expression

Full-length *COP1*, *SPAs* (*SPA2* to *SPA4*), *UVR8*, *HY5*, *RUP1*, and *RUP2* were amplified from the *Arabidopsis thaliana* cDNA library. *SPA1* was codon-optimized for the mammalian cell expression system (GenScript). The truncated *SPAs* (*SPA1* to *SPA4*) and *UVR8* were subcloned using the standard polymerase chain reaction (PCR) method. All site-directed mutagenesis of *COP1*, *UVR8*, and *RUP2* were carried out using the Fusion PCR method. All the gene fragments were subcloned into a modified pMlink vector (*48*). For protein expression, full-length wild-type or mutated COP1 were fused with N-terminal 3×Flag tandem affinity tag. Full-length wild-type or mutated SPAs were fused with C-terminal His tag. RUP1, RUP2, and RUP2 mutants contained C-terminal 3×Flag tandem affinity tags. UVR8 and UVR8 mutants were fused with C-terminal twin-Strep II affinity tag. Expi293F (Invitrogen) was used for protein expression and routinely cultured in Union-293 medium [Union-Biotech (Shanghai) Co. Ltd.] under the following conditions: 5% CO_2, 37°C, and 110 rpm. pMlink plasmids encoding COP1 and SPA4$^{1–464}$ were cotransfected in the cells with polyethylenimines (Polysciences). The transfected cells were cultured for 60 hours before harvesting. The cells were collected by centrifugation at 2000*g* for 15 min. The cell pellet was washed with phosphate-buffered saline and resuspended in lysis buffer A containing 50 mM tris-HCl (pH 8.0) and 150 mM NaCl. The cell suspension was flash-frozen in liquid nitrogen and stored at −80°C.

UVR8 and *UVR8* mutants were also subcloned into the pET15 vector with an N-terminal 6×His tag. *HY5* was subcloned into the pET21 vector with a C-terminal 6×His tag. The fusion proteins were expressed in *E. coli* cell strain BL21 (DE3) as previously described (*49*).

Protein purification

The COP1-SPA4$^{1–464}$ complex was extracted from stored cell pellets. The cell suspension was thawed and lysed using a JN-02 homogenizer (JNBIO, China). The lysed cells were ultracentrifuged at 14,000 rpm at 4°C for 1 hour to remove the insoluble component. The supernatant was incubated with an anti-Flag G1 affinity resin (GenScript) at 4°C for 2 hours. The resin was washed with 20-bed volumes of buffer A and eluted with buffer A with 3×Flag peptide (300 μg ml^{-1}) (GenScript). The eluted protein was further purified

by a HiTrap Heparin HP column (GE Healthcare). The protein was concentrated with a 50-kDa-cutoff Centricon (Millipore) and further subjected to Superose 6 Increase 10/300 GL column (GE Healthcare) using the size exclusion chromatography A (SEC-A) buffer containing 25 mM tris-HCl (pH 8.0), 150 mM NaCl, and 5 mM dithiothreitol (DTT). The peak fractions were pooled and immediately used for the reconstitution of COP1-SPA4$^{1–464}$-UVR8 or COP1-SPA4$^{1–464}$-HY5 complexes, in which the UVR8 and HY5 were expressed in *E. coli* cell strain BL21 (DE3) and purified as previously described (stored in the SEC buffer) (*49*).

Assembly of COP1-SPA4$^{1–464}$-UVR8 complex

Purified COP1-SPA4$^{1–464}$ protein was mixed with UV-B–treated UVR8 at a molar ratio of 1:1.5 in SEC-A buffer. The reaction mixture was incubated at 4°C for 30 min followed by gel filtration on a Superose 6 increase 10/300 GL column (GE Healthcare Life Sciences) in SEC-A buffer. Fractions containing COP1-SPA4$^{1–464}$-UVR8 complexes were pooled for further biochemical assay.

Competitive binding assay

The COP1-SPA4$^{1–464}$-HY5 complex was assembled using the method described above in SEC-B buffer containing 25 mM tris-HCl (pH 8.0), 200 mM NaCl, and 5 mM DTT. The COP1-SPA4$^{1–464}$-HY5 proteins were mixed with UV-B–treated wild-type UVR8 or UVR8 variants (UVR8$^{VP/AA}$, UVR8^{D44A,D77A,D129A}, and UVR8^{R234A,R286A,R338A}) at a molar ratio of 1:1.5 in SEC-B buffer. The reaction mixture was immediately analyzed by gel filtration on a Superose 6 increase 10/300 GL column (GE Healthcare Life Sciences) in SEC-B buffer. Elution fractions (from 11.5 to 17.5 ml) were pooled and analyzed by SDS–polyacrylamide gel electrophoresis (SDS-PAGE).

Gel filtration chromatography analysis

For gel filtration chromatography analysis, samples [except for the gradient fixation (GraFix) sample preparation; see the "Gradient fixation" section] were injected into a Superose-6 increase 10/300 GL column equilibrated with SEC-A buffer (for the assembly of COP1-SPA4$^{1–464}$-UVR8) and SEC-B buffer (for the assembly of COP1-SPA4$^{1–464}$-HY5 and the following competitive binding assay). Data analysis was carried out using GraphPad Prism 8.

Gradient fixation

The COP1-SPA4$^{1–464}$-UVR8 complex was cross-linked and purified using GraFix (*50*). The COP1-SPA4$^{1–464}$-UVR8 complex was first exchanged in GraFix buffer [25 mM Hepes (pH 7.5), 150 mM NaCl, and 5 mM DTT] and then loaded onto a 12-ml linear 10 to 30% (v/v) glycerol gradient in GraFix buffer supplemented with 0.05% EM-grade glutaraldehyde. After centrifugation at 4°C for 18 hours at 33,000 rpm in an SW40Ti rotor (Beckman Coulter), the sample was fractionated from top to bottom using the Piston Gradient Fractionator (Biocomp), and the cross-linking reactions were quenched with 74 mM tris-HCl (pH 8.0). Peak fractions were pooled and loaded onto a HiTrap desalting column (GE Healthcare Life Sciences) pre-equilibrated with GraFix buffer to remove the glycerol and concentrated to approximately 0.55 mg ml^{-1}.

Cryo-EM grid preparation and data collection

For cryo-EM sample preparation, a 3-μl aliquot of the GraFixed COP1-SPA4$^{1–464}$-UVR8 complex (~0.55 mg ml^{-1}) was dropped onto glow-discharged holey carbon grids (Quantifoil Au R1.2/1.3, 300 mesh), blotted with a Vitrobot Mark IV (Thermo Fisher Scientific) using 3.5-s blotting time with 100% humidity at 8°C, and plunged into liquid ethane cooled by liquid nitrogen. Cryo-EM data were collected on the FEI Titan Krios at 300 kV equipped with a K3 summit direct detector (Gatan) and a Gatan imaging filter (GIF) quantum energy filter (Gatan) operated with a slit width of 15 eV. *E Pluribus Unum* (EPU) was used for fully automated data collection with a nominal magnification of 105,000×, resulting in a pixel size of 0.827 Å per pixel. Image stacks of 40 movie frames were collected in super-resolution mode with a preset defocus range from −1.0 to −1.5 μm and a dose rate of 1.25 e^{-}/Å^2 per frame. A total of 4002 image stacks were collected for the COP1-SPA4$^{1–464}$-UVR8 complex. All image stacks were motion-corrected using MotionCor2 with a binning factor of 2 with dose weighting (*51*). The defocus values were estimated using Gctf (*52*).

Cryo-EM data processing, model building, and refinement

The schematic of the data processing pipeline is shown in fig. S3. About 4,073,221 particles from 3928 micrographs were automatically picked using the cryoSPARC blob picker (*53*). After two-dimensional (2D) classification, a total of 3,495,943 good particles were selected and subjected to several cycles of 3D classification in cryoSPARC (*53*). Particles belonging to the best class were selected; this is followed by nonuniform refinement and local refinement. The COP1^{WD40}-UVR8 complex yielded a cryo-EM density with an estimated resolution of 3.1 Å based on gold standard Fourier shell correlation (*54*).

For the atomic model of the COP1^{WD40}-UVR8 complex, the structures of UVR8$^{406–411}$-COP1^{WD40} (6QTQ) (*19*) and wild-type UVR8 (4DNW) (*26*) were rigidly docked into the density map and manually adjusted using COOT (*55*). This model was refined against the map using PHENIX in real space with secondary structure and geometry restraints (*56*). Model quality was evaluated using the MolProbity scores (*57*) and the Ramachandran plots (table S1).

The density for the UVR8 core domain, COP1^{WD40}, and the VP motif of UVR8 binding to COP1^{WD40} were observed, while the N-terminal domains of COP1 (1 to 350) and SPA4$^{1–464}$ (1 to 464) were missing, probably because of flexibility. Residues 365 to 371 and 632 to 642 in COP1^{WD40}, as well as residues 1 to 12 in the N terminus and most C termini [382 to 440, except for the VP motif (406 to 412)] of UVR8 failed to be built because of poor density.

UV-B treatment of UVR8 and the redimerization of UVR8 mediated by RUP2

Before in vitro biochemical assays, the full-length wild-type and mutant UVR8 proteins were exposed to UV-B irradiation at 50-cm intervals using a UV-B lamp [narrowband Philips TL20W/01RS (0.26 mW/cm^2)] on ice for 30 min. After 30 min of UV-B irradiation, the dimeric UVR8 dissociated into active monomers. For the redimerization of UVR8 mediated by RUP2, RUP2 protein was immediately added to the reaction in the dark. The proteins were left at room temperature (25°C) to restore to their inactivate ground state in the absence of UV-B. An equal volume of the reaction products was sampled at various time points and subjected to SDS-PAGE.

In vitro pull-down assay

The Expi293F cells expressing wild-type/mutant UVR8-Strep II proteins were lysed in lysis buffer B [100 mM tris-HCl (pH 8.0), 150 mM NaCl, and 1 mM EDTA] by repeated freeze-thaw for three

times. The supernatant was incubated with Strep-Tactin IBA Lifesciences (IBA) affinity resin at 4°C for 2 hours. The bound proteins were washed with 50-bed volumes of buffer B and eluted with buffer B containing 2.5 mM D-desthiobiotin (IBA) after 30 min of incubation. The cells expressing wild-type/mutant Flag-COP1 in complex with $SPA4^{1–464}$ proteins were lysed in buffer A. The proteins were purified using anti-Flag G1 affinity resin (GenScript). The bound proteins were washed with 50-bed volumes of buffer A and eluted in buffer A containing Flag peptide (300 μg ml^{-1}) (GenScript) after 30 min of incubation.

The in vitro pull-down assays were performed as previously described (*58*). For in vitro Flag pull-down assays, the mixture of 100 μg of COP1-$SPA4^{1–464}$ and 100 μg of wild-type/mutant UVR8 was incubated with 100 μl of anti-Flag G1 affinity resin (GenScript) in buffer A at 4°C for 2 hours. The mixture was then purified using the Flag-tag protein purification method mentioned above. For in vitro Strep pull-down assays, 100 μg of UVR8 and 100 μg of wild-type/mutant COP1 in complex with $SPA4^{1–464}$ were incubated with 100 μl of Strep-Tactin (IBA Lifesciences) affinity resin in buffer B at 4°C for 2 hours. The mixture was then purified using the Strep II-tag protein purification method mentioned above. The input and elution samples were analyzed by SDS-PAGE.

Immunoblot and co-immunoprecipitation assays

The Expi293F cells coexpressing $UVR8^{W285}$ and wild-type/mutant RUP2 were lysed in lysis buffer B and were purified using the Strep II-tag protein purification method mentioned above. Proteins in the supernatant sample were detected by immunoblots with antibodies against Strep or Flag (all antibodies were used at 1:3000 dilution). Proteins from elution fractions were analyzed by SDS-PAGE and visualized with Coomassie blue staining.

SUPPLEMENTARY MATERIALS

Supplementary material for this article is available at https://science.org/doi/10.1126/sciadv.abn3337

View/request a protocol for this paper from *Bio-protocol*.

REFERENCES AND NOTES

1. X. Han, X. Huang, X. W. Deng, The photomorphogenic central repressor COP1: Conservation and functional diversification during evolution. *Plant Commun* **1**, 100044 (2020).
2. R. Podolec, E. Demarsy, R. Ulm, Perception and signaling of ultraviolet-B radiation in plants. *Annu. Rev. Plant Biol.* **72**, 793–822 (2021).
3. R. Podolec, R. Ulm, Photoreceptor-mediated regulation of the COP1/SPA E3 ubiquitin ligase. *Curr. Opin. Plant Biol.* **45**, 18–25 (2018).
4. M. C. Cheng, P. K. Kathare, I. Paik, E. Huq, Phytochrome signaling networks. *Annu. Rev. Plant Biol.* **72**, 217–244 (2021).
5. Q. Wang, C. Lin, Mechanisms of cryptochrome-mediated photoresponses in plants. *Annu. Rev. Plant Biol.* **71**, 103–129 (2020).
6. O. S. Lau, X. W. Deng, The photomorphogenic repressors COP1 and DET1: 20 years later. *Trends Plant Sci.* **17**, 584–593 (2012).
7. J. Ponnu, U. Hoecker, Illuminating the COP1/SPA ubiquitin ligase: Fresh insights into its structure and functions during plant photomorphogenesis. *Front. Plant Sci.* **12**, 662793 (2021).
8. X. W. Deng, M. Matsui, N. Wei, D. Wagner, A. M. Chu, K. A. Feldmann, P. H. Quail, COP1, an Arabidopsis regulatory gene, encodes a protein with both a zinc-binding motif and a G beta homologous domain. *Cell* **71**, 791–801 (1992).
9. C. Yi, X. W. Deng, COP1—From plant photomorphogenesis to mammalian tumorigenesis. *Trends Cell Biol.* **15**, 618–625 (2005).
10. L. H. Ang, S. Chattopadhyay, N. Wei, T. Oyama, K. Okada, A. Batschauer, X. W. Deng, Molecular interaction between COP1 and HY5 defines a regulatory switch for light control of Arabidopsis development. *Mol. Cell* **1**, 213–222 (1998).
11. M. T. Osterlund, C. S. Hardtke, N. Wei, X. W. Deng, Targeted destabilization of HY5 during light-regulated development of Arabidopsis. *Nature* **405**, 462–466 (2000).
12. U. Hoecker, P. H. Quail, The phytochrome A-specific signaling intermediate SPA1 interacts directly with COP1, a constitutive repressor of light signaling in Arabidopsis. *J. Biol. Chem.* **276**, 38173–38178 (2001).
13. Y. Saijo, J. A. Sullivan, H. Wang, J. Yang, Y. Shen, V. Rubio, L. Ma, U. Hoecker, X. W. Deng, The COP1-SPA1 interaction defines a critical step in phytochrome a-mediated regulation of HY5 activity. *Genes Dev.* **17**, 2642–2647 (2003).
14. S. Laubinger, K. Fittinghoff, U. Hoecker, The SPA quartet: A family of WD-repeat proteins with a central role in suppression of photomorphogenesis in arabidopsis. *Plant Cell* **16**, 2293–2306 (2004).
15. D. Zhu, A. Maier, J.-H. Lee, S. Laubinger, Y. Saijo, H. Wang, L.-J. Qu, U. Hoecker, X. W. Deng, Biochemical characterization of Arabidopsis complexes containing CONSTITUTIVELY PHOTOMORPHOGENIC1 and SUPPRESSOR OF PHYA proteins in light control of plant development. *Plant Cell* **20**, 2307–2323 (2008).
16. H. Chen, X. Huang, G. Gusmaroli, W. Terzaghi, O. S. Lau, Y. Yanagawa, Y. Zhang, J. Li, J.-H. Lee, D. Zhu, X. W. Deng, Arabidopsis CULLIN4-damaged DNA binding protein 1 interacts with CONSTITUTIVELY PHOTOMORPHOGENIC1-SUPPRESSOR OF PHYA complexes to regulate photomorphogenesis and flowering time. *Plant Cell* **22**, 108–123 (2010).
17. X. Huang, X. Ouyang, P. Yang, O. S. Lau, L. Chen, N. Wei, X. W. Deng, Conversion from CUL4-based COP1-SPA E3 apparatus to UVR8-COP1-SPA complexes underlies a distinct biochemical function of COP1 under UV-B. *Proc. Natl. Acad. Sci. U.S.A.* **110**, 16669–16674 (2013).
18. U. Hoecker, J. M. Tepperman, P. H. Quail, SPA1, a WD-repeat protein specific to phytochrome a signal transduction. *Science* **284**, 496–499 (1999).
19. M. Holm, C. S. Hardtke, R. Gaudet, X. W. Deng, Identification of a structural motif that confers specific interaction with the WD40 repeat domain of Arabidopsis COP1. *EMBO J.* **20**, 118–127 (2001).
20. K. Lau, R. Podolec, R. Chappuis, R. Ulm, M. Hothorn, Plant photoreceptors and their signaling components compete for COP1 binding via VP peptide motifs. *EMBO J.* **38**, e102140 (2019).
21. J. Ponnu, T. Riedel, E. Penner, A. Schrader, U. Hoecker, Cryptochrome 2 competes with COP1 substrates to repress COP1 ubiquitin ligase activity during *Arabidopsis* photomorphogenesis. *Proc. Natl. Acad. Sci. U.S.A.* **116**, 27133–27141 (2019).
22. J.-J. Favory, A. Stec, H. Gruber, L. Rizzini, A. Oravecz, M. Funk, A. Albert, C. Cloix, G. I. Jenkins, E. J. Oakeley, H. K. Seidlitz, F. Nagy, R. Ulm, Interaction of COP1 and UVR8 regulates UV-B-induced photomorphogenesis and stress acclimation in Arabidopsis. *EMBO J.* **28**, 591–601 (2009).
23. X. Huang, P. Yang, X. Ouyang, L. Chen, X. W. Deng, Photoactivated UVR8-COP1 module determines photomorphogenic UV-B signaling output in Arabidopsis. *PLOS Genet.* **10**, e1004218 (2014).
24. R. Yin, A. B. Arongaus, M. Binkert, R. Ulm, Two distinct domains of the UVR8 photoreceptor interact with COP1 to initiate UV-B signaling in Arabidopsis. *Plant Cell* **27**, 202–213 (2015).
25. J. M. Christie, A. S. Arvai, K. J. Baxter, M. Heilmann, A. J. Pratt, A. O. 'Hara, S. M. Kelly, M. Hothorn, B. O. Smith, K. Hitomi, G. I. Jenkins, E. D. Getzoff, Plant UVR8 photoreceptor senses UV-B by tryptophan-mediated disruption of cross-dimer salt bridges. *Science* **335**, 1492–1496 (2012).
26. D. Wu, Q. Hu, Z. Yan, W. Chen, C. Yan, X. Huang, J. Zhang, P. Yang, H. Deng, J. Wang, X. W. Deng, Y. Shi, Structural basis of ultraviolet-B perception by UVR8. *Nature* **484**, 214–219 (2012).
27. L. Rizzini, J.-J. Favory, C. Cloix, D. Faggionato, A. O. Hara, E. Kaiserli, R. Baumeister, E. Schäfer, F. Nagy, G. I. Jenkins, R. Ulm, Perception of UV-B by the Arabidopsis UVR8 protein. *Science* **332**, 103–106 (2011).
28. G. I. Jenkins, The UV-B photoreceptor UVR8: From structure to physiology. *Plant Cell* **26**, 21–37 (2014).
29. C. Cloix, E. Kaiserli, M. Heilmann, K. J. Baxter, B. A. Brown, A. O. 'Hara, B. O. Smith, J. M. Christie, G. I. Jenkins, C-terminal region of the UV-B photoreceptor UVR8 initiates signaling through interaction with the COP1 protein. *Proc. Natl. Acad. Sci. U.S.A.* **109**, 16366–16370 (2012).
30. M. Binkert, L. Kozma-Bognár, K. Terecskei, L. De Veylder, F. Nagy, R. Ulm, UV-B-responsive association of the Arabidopsis bZIP transcription factor ELONGATED HYPOCOTYL5 with target genes, including its own promoter. *Plant Cell* **26**, 4200–4213 (2014).
31. M. Heijdea, M. Binkerta, R. Yina, F. Ares-Orpela, L. Rizzinib, E. Van De Slijkec, G. Persiauc, J. Nolfc, K. Gevaerte, G. De Jaegerc, R. Ulm, Constitutively active UVR8 photoreceptor variant in *Arabidopsis*. *Proc. Natl. Acad. Sci. U.S.A.* **110**, 20326–20331 (2013).
32. R. Podolec, K. Lau, T. B. Wagnon, M. Hothorn, R. Ulm, A constitutively monomeric UVR8 photoreceptor confers enhanced UV-B photomorphogenesis. *Proc. Natl. Acad. Sci. U.S.A.* **118**, (2021).
33. M. Heijde, R. Ulm, Reversion of the Arabidopsis UV-B photoreceptor UVR8 to the homodimeric ground state. *Proc. Natl. Acad. Sci. U.S.A.* **110**, 1113–1118 (2013).
34. H. Gruber, M. Heijde, W. Heller, A. Albert, H. K. Seidlitz, R. Ulm, Negative feedback regulation of UV-B-induced photomorphogenesis and stress acclimation in Arabidopsis. *Proc. Natl. Acad. Sci. U.S.A.* **107**, 20132–20137 (2010).

35. S. Uljon, X. Xu, I. Durzynska, S. Stein, G. Adelmant, J. A. Marto, W. S. Pear, S. C. Blacklow, Structural basis for substrate selectivity of the E3 ligase COP1. *Structure* **24**, 687–696 (2016).
36. A. M. Weissman, N. Shabek, A. Ciechanover, The predator becomes the prey: Regulating the ubiquitin system by ubiquitylation and degradation. *Nat. Rev. Mol. Cell Biol.* **12**, 605–620 (2011).
37. V. Balaji, T. Hoppe, Regulation of E3 ubiquitin ligases by homotypic and heterotypic assembly. *F1000Res* **9**, F1000 (2020).
38. M. V. Poyurovsky, C. Priest, A. Kentsis, K. L. B. Borden, Z.-Q. Pan, N. Pavletich, C. Prives, The Mdm2 RING domain C-terminus is required for supramolecular assembly and ubiquitin ligase activity. *EMBO J.* **26**, 90–101 (2007).
39. S. Uldrijan, W. J. Pannekoek, K. H. Vousden, An essential function of the extreme C-terminus of MDM2 can be provided by MDMX. *EMBO J.* **26**, 102–112 (2007).
40. A. Rojas-Fernandez, A. Plechanovová, N. Hattersley, E. Jaffray, M. H. Tatham, R. T. Hay, SUMO chain-induced dimerization activates RNF4. *Mol. Cell* **53**, 880–892 (2014).
41. A. Plechanovová, E. G. Jaffray, S. A. McMahon, K. A. Johnson, I. Navrátilová, J. H. Naismith, R. T. Hay, Mechanism of ubiquitylation by dimeric RING ligase RNF4. *Nat. Struct. Mol. Biol.* **18**, 1052–1059 (2011).
42. H. Dou, L. Buetow, G. J. Sibbet, K. Cameron, D. T. Huang, BIRC7-E2 ubiquitin conjugate structure reveals the mechanism of ubiquitin transfer by a RING dimer. *Nat. Struct. Mol. Biol.* **19**, 876–883 (2012).
43. P. D. Mace, K. Linke, R. Feltham, F.-R. Schumacher, C. A. Smith, D. L. Vaux, J. Silke, C. L. Day, Structures of the cIAP2 RING domain reveal conformational changes associated with ubiquitin-conjugating enzyme (E2) recruitment. *J. Biol. Chem.* **283**, 31633–31640 (2008).
44. L. Hu, J. Xu, X. Xie, Y. Zhou, P. Tao, H. Li, X. Han, C. Wang, J. Liu, P. Xu, D. Neculai, Z. Xia, Oligomerization-primed coiled-coil domain interaction with Ubc13 confers processivity to TRAF6 ubiquitin ligase activity. *Nat. Commun.* **8**, 814 (2017).
45. Q. Yin, S.-C. Lin, B. Lamothe, M. Lu, Y.-C. Lo, G. Hura, L. Zheng, R. L. Rich, A. D. Campos, D. G. Myszka, M. J. Lenardo, B. G. Darnay, H. Wu, E2 interaction and dimerization in the crystal structure of TRAF6. *Nat. Struct. Mol. Biol.* **16**, 658–666 (2009).
46. M. Heilmann, G. I. Jenkins, Rapid reversion from monomer to dimer regenerates the ultraviolet-B photoreceptor UV RESISTANCE LOCUS8 in intact Arabidopsis plants. *Plant Physiol.* **161**, 547–555 (2013).
47. H. Ren, J. Han, P. Yang, W. Mao, X. Liu, L. Qiu, C. Qian, Y. Liu, Z. Chen, X. Ouyang, X. Chen, X. W. Deng, X. Huang, Two E3 ligases antagonistically regulate the UV-B response in Arabidopsis. *Proc. Natl. Acad. Sci. U.S.A.* **116**, 4722–4731 (2019).
48. P. Lu, X.-C. Bai, D. Ma, T. Xie, C. Yan, L. Sun, G. Yang, Y. Zhao, R. Zhou, S. H. W. Scheres, Y. Shi, Three-dimensional structure of human γ-secretase. *Nature* **512**, 166–170 (2014).
49. L. Ma, X. Wang, Z. Guan, L. Wang, Y. Wang, L. Zheng, Z. Gong, C. Shen, J. Wang, D. Zhang, Z. Liu, P. Yin, Structural insights into BIC-mediated inactivation of Arabidopsis cryptochrome 2. *Nat. Struct. Mol. Biol.* **27**, 472–479 (2020).
50. B. Kastner, N. Fischer, M. M. Golas, B. Sander, P. Dube, D. Boehringer, K. Hartmuth, J. Deckert, F. Hauer, E. Wolf, H. Uchtenhagen, H. Urlaub, F. Herzog, J. M. Peters, D. Poerschke, R. Lührmann, H. Stark, GraFix: Sample preparation for single-particle electron cryomicroscopy. *Nat. Methods* **5**, 53–55 (2008).
51. S. Q. Zheng, E. Palovcak, J.-P. Armache, K. A. Verba, Y. Cheng, D. A. Agard, MotionCor2: Anisotropic correction of beam-induced motion for improved cryo-electron microscopy. *Nat. Methods* **14**, 331–332 (2017).
52. K. Zhang, Gctf: Real-time CTF determination and correction. *J. Struct. Biol.* **193**, 1–12 (2016).
53. A. Punjani, J. L. Rubinstein, D. J. Fleet, M. A. Brubaker, cryoSPARC: Algorithms for rapid unsupervised cryo-EM structure determination. *Nat. Methods* **14**, 290–296 (2017).
54. P. B. Rosenthal, R. Henderson, Optimal determination of particle orientation, absolute hand, and contrast loss in single-particle electron cryomicroscopy. *J. Mol. Biol.* **333**, 721–745 (2003).
55. P. Emsley, K. Cowtan, Coot: Model-building tools for molecular graphics. *Acta Crystallogr. D Biol. Crystallogr.* **60**, 2126–2132 (2004).
56. P. D. Adams, P. V. Afonine, G. Bunkóczi, V. B. Chen, I. W. Davis, N. Echols, J. J. Headd, L.-W. Hung, G. J. Kapral, R. W. Grosse-Kunstleve, A. J. Mc Coy, N. W. Moriarty, R. Oeffner, R. J. Read, D. C. Richardson, J. S. Richardson, T. C. Terwilliger, P. H. Zwart, PHENIX: A comprehensive Python-based system for macromolecular structure solution. *Acta Crystallogr. D Biol. Crystallogr.* **66**, 213–221 (2010).
57. I. W. Davis, A. Leaver-Fay, V. B. Chen, J. N. Block, G. J. Kapral, X. Wang, L. W. Murray, W. B. Arendall III, J. Snoeyink, J. S. Richardson, D. C. Richardson, MolProbity: All-atom contacts and structure validation for proteins and nucleic acids. *Nucleic Acids Res.* **35**, W375–W383 (2007).
58. Y. Yang, T. Liang, L. Zhang, K. Shao, X. Gu, R. Shang, N. Shi, X. Li, P. Zhang, H. Liu, UVR8 interacts with WRKY36 to regulate HY5 transcription and hypocotyl elongation in Arabidopsis. *Nat. Plants* **4**, 98–107 (2018).

Acknowledgments: We thank the Cryo-EM Facility of Southern University of Science and Technology for providing technical support during EM image acquisition and the Center for Protein Research and Public Laboratory of Electron Microscopy, Huazhong Agricultural University, for technical support, as well as Q. Wang and J. Cao for assistance during cryo-EM image acquisition and two anonymous reviewers whose comments have significantly improved this manuscript. **Funding:** This work was supported by funds from the Ministry of Science and Technology of China (2018YFA0507700 and 2017YFA0503800), the National Natural Science Foundation of China (31722017, 32071211, 31870753, and 31621001), the Wuhan Applied Foundational Frontier Project (2019020701011460), the Foundation of Hubei Hongshan Laboratory (2021hszd010), and Southern University of Science and Technology (Y01226026). **Author contributions:** P.Y. and X.W.D. conceived the project. Y.W., L.W., and P.Y. designed all experiments. Y.W., L.W., H.C., and L.Q. performed the experiments. Y.W. collected the EM data. Z.G. determined the structure. All authors analyzed the data and contributed to manuscript preparation. Y.W., L.W., and P.Y wrote the manuscript. **Competing interests:** The authors declare that they have no competing interests. **Data and materials availability:** The atomic coordinates and EM density for the reported structures of the COP1^{WD40}-UVR8 complex (PDB: 7VGG, EMDB: EMD-31968) have been deposited in the Protein Data Bank (www.rcsb.org). All data needed to evaluate the conclusions in the paper are present in the paper and/or the Supplementary Materials.

Submitted 18 November 2021
Accepted 4 March 2022
Published 20 April 2022
10.1126/sciadv.abn3337